Dalton Transactions

Impact of Ligand Chlorination and Counterion Tuning on High-Field Spin Relaxation in a Series of V(IV) Complexes

Journal:	*Dalton Transactions*
Manuscript ID	DT-ART-04-2023-001274.R2
Article Type:	Paper
Date Submitted by the Author:	10-Jul-2023
Complete List of Authors:	Martinez, Roxanna; Colorado State University Department of Chemistry Jackson, Cassidy; Colorado State University, Chemistry Üngör, Ökten; Colorado State University Department of Chemistry van Tol, Johan; Florida State University, National High Magnetic Field Laboratory Zadrozny, Joseph; Colorado State University, Chemistry

ARTICLE

Impact of Ligand Chlorination and Counterion Tuning on High-Field Spin Relaxation in a Series of V(IV) Complexes

Received 00th January 20xx,
Accepted 00th January 20xx

DOI: 10.1039/x0xx00000x

Roxanna Martinez,*[a] Cassidy E. Jackson,[a] Ökten Üngör,[a] Johan van Tol[b] and Joseph M. Zadrozny *[a]

Methods of controlling spin coherence by molecular design are essential to efforts to develop molecular qubits for quantum information and sensing applications. In this manuscript, we perform the first studies of how arrangements of $^{35/37}$Cl nuclear spins in the ligand shell and counterion selection affect the coherent spin dynamics of V(IV) complexes at high magnetic field. We prepared eight derivatives of the vanadium triscatecholate complex with varying arrangements of $^{35/37}$Cl substitution on the catechol backbone and R_3NH^+ counterions (R = Et, *n*-Bu, *n*-Hex) and investigated these species via structural and spectroscopic methods. Hahn-echo pulsed electron paramagnetic resonance (EPR) experiments at high-frequency (120 GHz) and field (*ca*. 4.4 T) were used to extract the phase-memory relaxation time (T_m) and spin-lattice relaxation (T_1) times of the series of complexes. We found T_m values ranging from 4.8 to 1.1 μs in the temperature range of 5 to 40 K, varying by approximately 20% as a function of substitutional pattern. In-depth analysis of the results herein and comparison with related studies of brominated analogues disprove multiple hypothesized mechanisms for T_m control. Ultimately, we propose that more specific properties of the halogen atoms, e.g. the chemical shift, V•••Cl hyperfine coupling, and quadrupolar coupling, could be contributing to the V(IV) T_m time.

Introduction

Magnetic molecules are promising candidates for a wide variety of spin-based applications, including qubit development, information storage, and magnetic resonance imaging.[1-4] Toward these applications, understanding how to control and lengthen spin-relaxation by design of the spin system is important. Here, molecular complexes possessing open-shell metal ions play an important role because synthetic design of ligand shell, metal ion, or oxidation state can be used to tune and slow relaxation times.[5,6] Important results stemmed from these efforts, including, e.g. millisecond spin-spin relaxation times or magnetic hysteresis above liquid N_2 temperatures.[7-10]

One persistent challenge in controlling relaxation is the control of phase-memory relaxation or decoherence, indicated by the phase-memory relaxation time, T_m, (also frequently called T_2, the spin-spin relaxation time, or coherence time in the literature) in magnetic, noisy environments. Environments of this type interact with embedded spins and hasten relaxation, often by orders of magnitude.[11-12] Thus, the prevailing strategies require complete elimination of these environments, either by nuclear-spin-free synthetic design or isolation in isotopically purified environments.[7,13-15]

Recently, we demonstrated that the effective "environment" of a magnetic complex can be the molecule itself. Variable counterion studies showed that the type of magnetic nucleus in the molecule (e.g., the difference between methyl ^{1}H and aromatic or aliphatic ^{1}H), not sheerly the number, can dictate phase-memory relaxation.[16] We also showed that changing the position of magnetic nuclei can be impactful, such that ligands with the same chemical composition, but different nuclear spin arrangements, or "patterns", will affect T_m.[17] This latter effort was inspired by justifications for the long coherence times for the vacancies in SiC.[18-19] These studies suggested that magnetic nuclei in the ligand shell are powerful controllers of spin relaxation, in contrast to theories that had previously assumed such nuclei were deactivated from causing noise owing to hyperfine interactions. The foregoing observations were thus significant for showing that ligand-based nuclei can play a role in electron spin relaxation. In this new paradigm, one can consider the ligand shell as being an overwhelmingly influential "edge" of the local magnetic environment, capable of overriding the effects of magnetic noise from the solvent.[13]

If the ligand shell and counterion are indeed the dominant factors governing relaxation, we need far deeper understanding of how different types and arrangements of nuclei affect relaxation. In a previous study, some of us reported that different patterns of ^{1}H (*I*

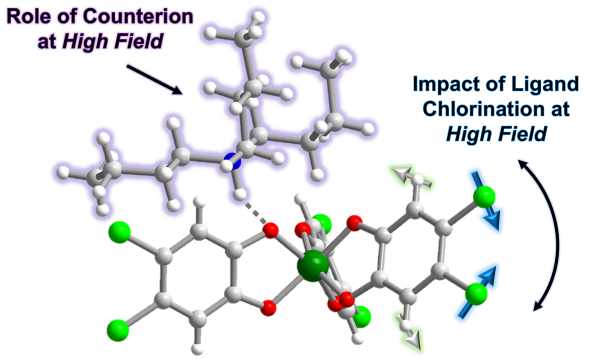

Figure 1. Overview of strategies for controlling phase memory relaxation (T_m) via molecular design being investigated.

[a] Department of Chemistry, Colorado State University, Fort Collins, CO 80523, USA. E-mail: joe.zadrozny@colostate.edu
[b] National High Magnetic Field Laboratory, Tallahassee, FL 32310, USA
† Electronic Supplementary Information (ESI) available: Additional characterization. CCDC 2158535, 2159088, 2159051. See DOI: 10.1039/x0xx00000x

= 1/2, 2.79 μ_N) and $^{79/81}$Br (^{79}Br: I = 3/2, 2.11 μ_N; ^{81}Br: I = 3/2, 2.27 μ_N) magnetic nuclei in the ligand shell can produce up to 50 % variation in T_m at high field/frequency (Fig. 1).[17,20] In that original paper, we proposed a mechanism where symmetric ligands shorten T_m by enabling efficient spin diffusion for the ^{1}H atoms in the ligand shell. The symmetry of the ligands is essential in this context, as nuclei require the same resonant frequency (or chemical shift) to engage in spin diffusion, and symmetric ligands enforce that outcome.

That aforementioned study left behind three key questions. First, simply, is spin diffusion in ligand ^{1}H atoms truly responsible for suppressing T_m? An alternative hypothesis is that the $^{79/81}$Br ligand nuclei are engaging in this behavior (or are otherwise deleterious to T_m), as these nuclei are also symmetrically arranged in any catecholate ligand where the protons are. Second, in the aforementioned study, the unique, short-T_m species, $[V(C_6H_2\text{-}4,5\text{-}Br_2O_2)_3]^{2-}$ (C_6H_2-4,5-Br_2O_2) = 4,5-dibromocatecholate) exhibited a geometry that was closer to trigonal prismatic symmetry when all other complexes were slightly closer to octahedral geometry. Thus, was the interpretation of a ligand nuclear spin effect wrong, and instead a slight change in geometry around the V(IV) ion is responsible? Finally, third, could the difference instead be related to the counterion? Our prior work showed that, at X-band frequencies and lower fields, the CH_3 groups of the R_3NH^+ counterions dictate T_m, as they are strong enough to override environmental deuteration effects.[16,17,21] Our initial motivation for high-field studies of the brominated complexes was to decouple the EPR transition from the frequency of CH_3 rotation (< 10 MHz).[15,17,22] Yet, the counterion dependence of T_m at high frequency has never been tested as a control.

To resolve these questions, we prepared a set of six V(IV) complexes with varying substitutional patterns of $^{35/37}$Cl nuclear spins on the ligand shell, $(n\text{-}Bu_3NH)_2[V(C_6H_{4-x}Cl_xO_2)_3]$ (Complexes **1**-**6**, Figs. 1 and 2), and two additional complexes, $(Et_3NH)_2[V(C_6H_4O_2)_3]$ (**7**) and $(n\text{-}Hex_3NH)_2[V(C_6H_4O_2)$ (**8**), and investigated their dynamic electronic spin properties via magnetic resonance. We hypothesized the following. First, observation of the exact same trend as with $^{79/81}$Br-functionalized complexes, would pinpoint ^{1}H protons as the source of decoherence. Second, that a trend in structures would be isolated, enabling us to rule out a unique structural distortion as an alternative mechanism of the abnormally fast T_m relaxation in $[V(C_6H_2\text{-}4,5\text{-}Br_2O_2)_3]^{2-}$. Third, the important counterion analyses would provide a vital control for the observed effects. We reasoned that all of these data and comparison of the $^{79/81}$Br v. $^{35/37}$Cl series would help shed light on the larger role of ligand nuclear spins on electron spin relaxation in metal complexes.

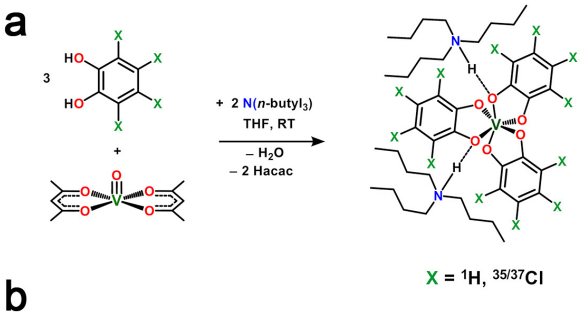

b

Ligand	Complex Formula and Label
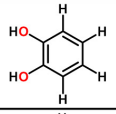	$(n\text{-}Bu_3NH)_2[V(C_6H_4O_2)_3]$ **1**
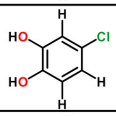	$(n\text{-}Bu_3NH)_2[V(C_6H_2\text{-}4\text{-}Cl_2O_2)_3]$ **2**
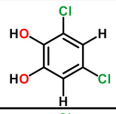	$(n\text{-}Bu_3NH)_2[V(C_6H_2\text{-}3,5\text{-}Cl_2O_2)_3]$ **3**
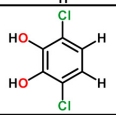	$(n\text{-}Bu_3NH)_2[V(C_6H_2\text{-}3,6\text{-}Cl_2O_2)_3]$ **4**
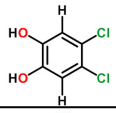	$(n\text{-}Bu_3NH)_2[V(C_6H_2\text{-}4,5\text{-}Cl_2O_2)_3]$ **5**
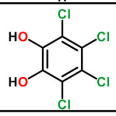	$(n\text{-}Bu_3NH)_2[V(C_6Cl_4O_2)_3]$ **6**
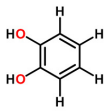	$(Et_3NH)_2[V(C_6H_4O_2)_3]$ **7**
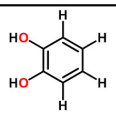	$(n\text{-}Hex_3NH)_2[V(C_6H_4O_2)_3]$ **8**

Figure 2. Synthetic scheme and complexes. (**a**) The general synthetic scheme to produce the studied V(IV) complexes is depicted. (**b**) The series of six ligands used in this study and associated formulae for the metal complexes **1**-**8**.

Experimental

General Considerations. The complex $(n\text{-}Bu_3NH)_2[V(C_6H_4O_2)_3]$ (**1**) was reported to be air-sensitive.[23,24] Thus, all manipulations and syntheses of it and **2**–**6** were performed under a N_2 atmosphere with either a Vigor glovebox or Schlenk techniques. The complexes $(Et_3NH)_2[V(C_6H_4O_2)_3]$ (**7**) and $(n\text{-}Hex_3NH)_2[V(C_6H_4O_2)_3]$ (**8**) were prepared following published procedures.[16] Glassware was flame-dried before bringing into the glovebox. Tetrahydrofuran (THF), diethyl ether (Et_2O), and hexanes were dried using a commercial solvent purification system from LC Technology Solutions and were stored over 4 Å molecular sieves prior to use. 4 Å molecular sieves were stored in a 150 °C oven and were activated at 280 °C under reduced pressure for at least 12 h prior to use. THF, Et_2O, and hexanes were subjected to a test with a standard purple solution of sodium benzophenone ketyl in THF to confirm low O_2 and H_2O content. Triethylamine (Et_3N), tri-n-butylamine (n-Bu_3N), tri-n-hexylamine (n-Hex_3N), and hexamethyldisiloxane (HMDSO) were purchased from commercial suppliers and dried by stirring over CaH_2 for at least 24 h then distilled over CaH_2. Tetrachlorocatechol, 4-chlorocatechol, 4,5-dichlorocatechol, 3,6-dichlorocatehcol, vanadyl acetylacetonate ($VO(acac)_2$), and d^{14}-o-terphenyl were purchased from commercial suppliers and were used as received. 3,5-chlorocatechol was prepared following the literature procedures.[25]

Synthetic Procedures

$(n\text{-}Bu_3NH)_2[V(C_6H_3\text{-}4\text{-}ClO_2)_3]$ (2) In a N_2-filled glovebox, a 20-mL scintillation vial was charged with 0.110 g (0.412 mmol) $VO(acac)_2$, 0.178 g (1.23 mmol) 4-chlorocatechol, ca. 8 mL THF, and a Teflon-coated magnetic stir bar. A solution of 195 µL (0.823 mmol) n-Bu_3N

was added to the mixture with gentle shaking, resulting almost immediately in an intensely dark blue solution. The reaction mixture was allowed to stir overnight. All volatile materials (THF, H_2O, and acetylacetone) were removed under reduced pressure. The resulting dark blue residue was washed twice with ca. 5 mL cold Et_2O (Note: the complex is slightly soluble in Et_2O) and twice with ca. 5 mL hexanes and then was dried under reduced pressure to yield 0.342 g of dark blue powder. The solid was further purified by crystallization with slow evaporation of a THF mother liquor in a −35 °C freezer in the glovebox for 2-3 days to afford 0.334 g (0.392 mmol, 95 % yield) of large, shiny, dark blue crystals suitable for single-crystal X-ray diffraction. The ^{1}H NMR spectrum of **2** in $CDCl_3$ reveals extremely broadened signals that are depicted in Fig. S1. IR (KBr, cm^{-1}): 3065, 2958, 2930, 2871. 2632, 2556, 1558, 1466, 1379, 1256, 1216, 1106, 1055, 1023, 846, 792, 735, 637, 571, 502, 407. UV-vis (THF); λmax (εM, $M^{-1}cm^{-1}$): 298 (15000); 456 (3200); 575 (5200); 682 (4800). LTQ-MS (m/z): positive ion mode: {(n-Bu_3NH)$_3$[$V(C_6H_2ClO_2)$]}$^+$, 849.33 {n-Bu_3NH}$^+$, 186.22 (base). Combustion analyses calculated for $C_{42}H_{65}Cl_3N_2O_6V$ (found): 59.88 (59.26) % C; 7.38 (7.70) % H; 3.49 (3.29) % N.

(n-Bu_3NH)$_2$[$V(C_6H_2$-3,5-$Cl_2O_2)_3$] (3) In a N_2-filled glovebox, a 20-mL scintillation vial was charged with 0.136 g (0.509 mmol) $VO(acac)_2$, 0.273 g (1.52 mmol) 3,5-dichlorocatechol, ca. 8 mL THF, and a Teflon-coated magnetic stir bar. A solution of 238 µL (1.00 mmol) n-Bu_3N was added to the mixture with gentle shaking, resulting almost immediately in an intensely dark blue solution. The reaction mixture was allowed to stir overnight. All volatile materials (THF, H_2O, and acetylacetone) were removed under reduced pressure. The resulting dark blue residue was washed twice with ca. 5 mL cold Et_2O (Note: the complex is slightly soluble in Et_2O) and twice with ca. 5 mL hexanes and then was dried under reduced pressure to yield 0.431 g (0.451 mmol, 95 % yield) of dark blue powder. All crystallization attempts resulted in samples where crystals were too small for diffraction or amorphous solids. The ^{1}H NMR spectrum of **3** in $CDCl_3$ reveals extremely broadened signals that are depicted in Fig. S2. IR (KBr, cm^{-1}): 3095, 2961, 2929, 2870, 2732, 2656, 1667, 1554, 1448, 1406, 1381, 1305, 1257, 1229, 1099, 1077, 1018, 956, 860, 803, 761, 663, 606, 593, 535, 519, 488, 459, 425, 413, 403. UV-vis (THF); λmax (εM, $M^{-1}cm^{-1}$): 293 (15000); 391 (5000); 580 (8100); 682 (7200). LTQ-MS (m/z): positive ion mode: {n-Bu_3NH}$^+$, 186.22 (base); negative ion mode: {[$V(C_6H_2Cl_2O_2)_3$]}$^-$, 578.74. Combustion analyses calculated for $C_{42}H_{62}Cl_6N_2O_6V$ (found): 51.57 (52.84) % C; 6.62 (6.55) % H; 2.63 (2.93) % N.

(n-Bu_3NH)$_2$[$V(C_6H_2$-3,6-$Cl_2O_2)_3$] (4) In a N_2-filled glovebox, a 20-mL scintillation vial was charged with 0.133 g (0.497 mmol) $VO(acac)_2$, 0.268 g (1.53 mmol) 3,6-dichlorocatechol, ca. 8 mL THF, and a Teflon-coated magnetic stir bar. A solution of 238 µL (1.00 mmol) n-Bu_3N was added to the mixture with gentle shaking, resulting almost immediately in an intensely dark blue solution. The reaction mixture was allowed to stir overnight. All volatile materials (THF, H_2O, and acetylacetone) were removed under reduced pressure. The resulting dark blue residue was washed twice with ca. 5 mL cold Et_2O (Note: the complex is slightly soluble in Et_2O) and twice with ca. 5 mL hexanes and then was dried under reduced pressure to yield 0.405 g (0.424 mmol, 89 % yield) of dark blue powder. Crystallization attempts resulted in crystals too small for diffraction or amorphous solids. The ^{1}H NMR spectrum of **4** in $CDCl_3$ reveals extremely broadened signals that are depicted in Fig. S3**.** IR (KBr, cm^{-1}): 3064, 2959, 2930, 2870, 2672, 1558, 1527, 1452, 1420, 1379, 1297, 1240, 1162, 1115, 1051, 1028, 939, 918, 798, 758, 733, 684, 562, 521, 437, 425. UV-vis (THF); λmax (εM, $M^{-1}cm^{-1}$): 293 (11000); 576 (5000); 682 (46000). LTQ-MS (m/z): positive ion mode: {(n-Bu_3NH)$_3$[$V(C_6H_2Cl_2O_2)$]}$^+$, 961.21; {n-Bu_3NH}$^+$, 186.22 (base). Combustion analyses calculated for $C_{42}H_{62}Cl_6N_2O_6V$•$2C_4H_8O$ (found): 54.86 (54.65) % C; 6.75 (7.16) % H; 3.26 (2.90) % N.

(n-Bu_3NH)$_2$[$V(C_6H_2$-4,5-$Cl_2O_2)_3$] (5) In a N_2-filled glovebox, a 20-mL scintillation vial was charged with 0.132 g (0.494 mmol) $VO(acac)_2$, 0.265 g (1.48 mmol) 4,5-dichlorocatechol, ca. 8 mL THF, and a Teflon-coated magnetic stir bar. A solution of 234 µL (0.988 mmol) n-Bu_3N was added to the mixture with gentle shaking, resulting almost immediately in an intensely dark blue solution. The reaction mixture was allowed to stir overnight. All volatile materials (THF, H_2O, and acetylacetone) were removed under reduced pressure. The resulting dark blue residue was washed twice with ca. 5 mL cold Et_2O (Note: the complex is slightly soluble in Et_2O) and twice with ca. 5 mL hexanes and then was dried under reduced pressure to yield 0.438 g of dark blue powder. The solid was further purified by crystallization via slow evaporation of THF mother liquor in a −35 °C freezer in the glovebox for 2-3 days to afford 0.422 g (0.442 mmol, 89 % yield) of large, shiny, dark blue crystals suitable for single-crystal X-ray diffraction. The ^{1}H NMR spectrum of **5** in $CDCl_3$ reveals extremely broadened signals that are depicted in **Fig. S4.** IR (KBr, cm^{-1}): 3094, 2961, 2933, 2872, 2746, 2659, 2540, 1556, 1536, 1493, 1462, 1355, 1337, 1257, 1226, 1186, 1080, 1026, 919, 873, 850, 836, 802, 734, 674, 656, 602, 535, 472, 412, 408. UV-vis (THF); λmax (εM, $M^{-1}cm^{-1}$): 293 (11000); 579 (5100); 682 (45000). LTQ-MS (m/z): positive ion mode: {n-Bu_3NH}$^+$, 186.22 (base); negative ion mode: {[$V(C_6H_2Cl_2O_2)_3$]}$^-$, 578.74. Combustion analyses calculated for $C_{42}H_{62}Cl_6N_2O_6V$ (found): 52.87 (52.84) % C; 6.45 (6.55) % H; 3.05 (2.93) % N.

(n-Bu_3NH)$_2$[$V(C_6Cl_4O_2)_3$] (6) In a N_2-filled glovebox, a 20-mL scintillation vial was charged with 0.124 g (0.464 mmol) $VO(acac)_2$, 0.345 g (1.39 mmol) tetrachlorocatechol, and a Teflon-coated magnetic stir bar. A solution containing 0.220 µL (0.928 mmol) n-Bu_3N in 5 mL THF was added to the mixture with gentle shaking, resulting almost immediately in an intensely dark blue solution. The reaction mixture was allowed to stir overnight. All volatile materials (THF, H_2O, and acetylacetone) were removed under reduced pressure. The resulting dark blue residue was washed twice with ca. 5 mL Et_2O and then was dried under reduced pressure to yield 0.491 g of dark blue powder. The solid was further purified by crystallization with slow evaporation of THF mother liquor in a −35 °C freezer in the glovebox for 2-3 days to afford 0.478 g (0.411 mmol, 88% yield) of large, shiny, dark blue crystals suitable for single-crystal X-ray diffraction. The ^{1}H NMR spectrum of **6** in $CDCl_3$ reveals extremely broadened signals that are depicted in **Fig. S5.** IR (KBr, cm^{-1}): 3065, 2963, 2928, 2872, 1526, 1467, 1378, 1278, 1249, 1105, 977, 920, 807, 783, 739, 689, 565, 460. UV-vis (CH_3CN); λmax (εM, $M^{-1}cm^{-1}$): 293 (15000), 579 (8000), 684 (7200). LTQ-MS (m/z): positive ion mode: {n-Bu_3NH}$^+$, 186.25 (base); negative ion mode: {[$V(C_6Cl_4O_2)_3$]}$^-$, 789.53. Combustion analyses calculated for $C_{42}H_{56}Cl_{12}N_2O_6V$•$C_4H_8O$ (found): 44.80 (45.30) % C; 5.06 (5.23) % H; 2.27 (2.60) % N.

X-ray Data Collection, Structure Solution and Refinement

Single crystals were grown by placing a THF mother liquor of the desired complex into a smaller vial and placing it into a larger jar with HMDSO counter solvent. Presence of the counter solvent encouraged faster THF evaporation. Single-crystal diffraction data were collected at the X-Ray Diffraction facility of the Analytical Resources Core at Colorado State University. Data for **2** and **5** were collected on a Bruker D8 Quest ECO single-crystal X-ray diffractometer equipped with Mo Kα (λ = 0.71073 Å). Data for **6** were

collected at the X-ray diffraction facility at Cornell University. Data were collected and integrated using Bruker Apex 3 software. Absorption corrections were applied using SADABS.[26] Space group assignments were determined by examination of systematic absences, E-statistics, and successive refinement of the structures. Crystal structures were solved using SHELXT and refined with the aid of successive difference Fourier maps by SHELXL operated in conjunction with OLEX2 software.[27-30] None of the crystals demonstrated decay by X-ray radiation over the course of the experiment. Hydrogen atoms were placed in ideal positions and refined using a riding model for all structures. In **2** and **5** disordered THF was present and solvent mask was used in OLEX2 to model that disorder. See Tables S1-S3 for refinement details. Crystallographic information files for **2**, **5**, and **6** are available in the CSD at accession numbers 2158535, 2159088, 2159051.

Electron Paramagnetic Resonance

All samples were prepared under an inert atmosphere. For high-frequency analyses at the National High Magnetic Field Laboratory, samples **1**-**8** were prepared at 1 mM concentration by first loading 40 µL 1 mM THF solution of **1** by a micropipette into a 4 mm OD quartz EPR tube. Following removal of THF under reduced pressure, 0.0516 g d^{14}-o-terphenyl (40 µL when molten) was loaded into the same tube. These tubes were flame sealed under dynamic vacuum (< 50 mTorr) and placed in a 65−70 °C oil bath until a clear dark blue solution formed. While sample tubes prepared in this manner can be stored at room temperature for an extended period without compound decomposition, the quality of glass appeared to decay with extended time. Hence, prior to each measurement, the samples were remelted and frozen. For X-band continuous wave measurements, samples were prepared in toluene at 1 mM and flame sealed in 4 mm OD quartz tubes (Wilmad).

All continuous-wave EPR spectra were collected at the analytical resources core of Colorado State University with a Bruker ELEXSYS ESR-500 X-band CW EPR spectrometer. All pulsed EPR data were collected at the National High Magnetic Field Laboratory (NHMFL, Tallahassee, FL, USA). These data were collected on a custom built 120/240/336 GHz EPR spectrometer, operated at 120 GHz for the experiments in this paper.[31] Samples of **1**-**8** were gently melted using a heat gun to afford a homogeneous dark blue solution, then quickly inserted into the resonator to ensure glassing behavior of the OTP. Pulsed EPR data were processed using an EPR measurement program locally developed at NHMFL, Matlab 2018b, and Origin Pro 2018b software packages.[34] Continuous-wave and echo-detected, field-swept EPR spectra were simulated using Easyspin.[35] Note that for the solution-phase analyses, broadening was accounted for by modeling the data with the Garlic simulation method within Easyspin, which uses a correlation time (τ_c) to describe broadening of the EPR spectrum. This method has been used successfully in the past for analyzing solution phase V(IV) EPR spectra and, importantly, works only if the spin system is anisotropic (as they are here).

Spin-Lattice Relaxation Experiments and Analyses

T_1 data were collected on the most intense resonance of the EDFS spectra at 4.4 T at 120 GHz via an inversion recovery sequence (π – T – π/2 – τ – π – τ – echo). The length of the three pulses, π – π/2 – π, were 900– 600 – 900 ns with a starting T value of 10300 ns and τ of 700 ns. The inversion recovery data were fit using a stretched exponential function:[36]

$$\mathbf{I}(\boldsymbol{\tau}) = \boldsymbol{I}(\mathbf{0}) - \boldsymbol{A}\boldsymbol{e}^{-\left(\frac{\tau}{T_1}\right)^{\beta}} \quad (1)$$

The temperature dependent T_1 data were modeled with the following equation in Origin:

$$\frac{\mathbf{1}}{\boldsymbol{T_1}} = \boldsymbol{A}_{\mathbf{dir}}\boldsymbol{B}^{\mathbf{4}}\boldsymbol{T} + \boldsymbol{A}_{\mathbf{Ram}}\boldsymbol{T}^{\mathbf{9}} \quad (2)$$

Here, T is temperature, A_{dir} is the direct process coefficient, A_{ram} is the Raman process coefficient, and B is the magnetic field. The exponent of 4 was chosen for consistency with analyses of other V(IV) systems, and the Raman exponent of 9 was chosen for consistency with expectations for half-integer spins without low-lying excited states.[6,37]

Phase Memory Relaxation Experiments and Analyses

T_m data at 120 GHz were collected on the most intense resonance (4.4 T) in the EDFS spectra via a Hahn echo sequence (π/2 – τ – π – τ – echo) with a 4-step phase cycle with microwave pulses of 600 (π/2) and 900 ns (π) and an interpulse time (τ) of 700 ns. The Hahn echo decay data were fit using the stretched exponential equation:

$$\mathbf{I}(\boldsymbol{\tau}) = \boldsymbol{I}(\mathbf{0}) - \boldsymbol{A}\boldsymbol{e}^{-\left(\frac{2\tau}{T_m}\right)^{\beta}} \quad (3)$$

Here, β is the stretch parameter describing the shape of the echo decay.[18,38,39] The low temperature data were better fit with stretched exponential equation due to the dominant nuclear spin diffusion. We found that β approached 1 as the temperature increased, indicating that a conventional single exponential fit could be used. Nevertheless, we used the stretched exponential fit throughout the whole temperature range for consistency.

Owing to the long pulse lengths and 100 ns deadtime on the 120 GHz spectrometer, T_m values below 200-300 ns were in general extremely difficult to observe, hence all analyses generally stopped by 40 K. We also tested the dependence of T_m on the π-pulse length in the Hahn-echo sequence to test for the effects of instantaneous diffusion. A strong dependence of T_m on this pulse length indicates that instantaneous diffusion is integral to phase memory relaxation.[38] For these specific tests, echo decay curves were collected at 5 K and 120 GHz for **1**, **5** and the 4,5-dibromocatechol analogue of **5**, $(Bu_3NH)_2[V(C_6H_2Br_2O_2)_3]$, using a two-pulse Hahn echo sequence with a varied π -pulse length from 100 to 600 ns.

Other Physical Measurements

^{1}H NMR spectra were collected on a Bruker Avance NEO 400 MHz spectrometer. The spectra were referenced using residual protiated solvent signal as an internal standard ($CDCl_3$, 7.26 ppm). Combustion analyses were performed by Midwest Microlab (Indianapolis, IN, USA). Infrared spectra were recorded on a Bruker TENSOR II FTIR spectrometer. Electronic absorption spectra were recorded on acetonitrile solutions of **1**-**6** with a Hewlett-Packard 8453 spectrophotometer using air-free quartz cuvettes with a 1 cm path length. Linear trap quadrupole mass spectrometry (LTQ-MS) measurements were performed on acetonitrile solutions of **1**–**6** with a Thermo-Finnigan LTQ LC/MS-MS at the Analytical Resources Core (ARC) of Colorado State University.

Results

Preparation of the targeted complexes proceeded via simple one-pot reactions using $VO(acac)_2$, tri-*n*-butylamine, and the selected ligands (Fig. 2). All complexes were isolated as dark blue/purple compounds, and single crystals could generally be grown by slow evaporation of THF mother liquors, except for **3** and **4**. We speculate that ligand and

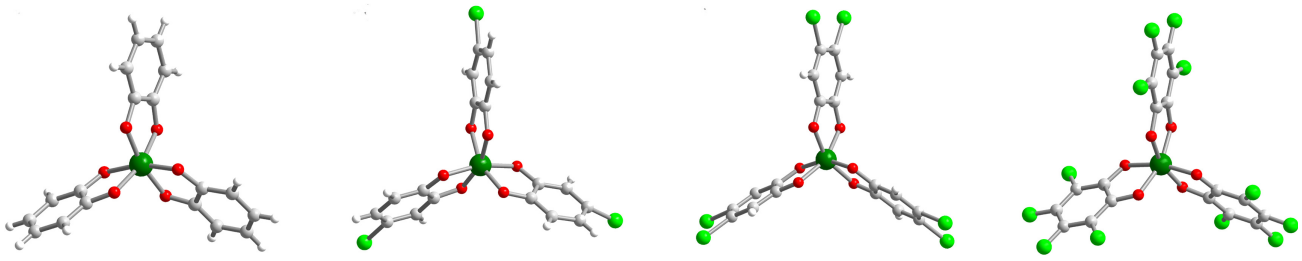

$[V(C_6H_4O_2)_3]^{2-}$ (1) $[V(C_6H_3ClO_2)_3]^{2-}$ (2) $[V(C_6H_2Cl_2O_2)_3]^{2-}$ (5) $[V(C_6Cl_4O_2)_3]^{2-}$ (6)

Figure 3. Molecular structures of the studied V(IV) complexes as determined in the crystal structures of **1**, **2**, **5**, and **6**. Hydrogen bonding contacts with the Bu_3NH^+ counterions are omitted for clarity. Dark green, light green, red, gray, and white spheres represent vanadium, chlorine, oxygen, carbon, and hydrogen atoms, respectively. Structure for **1** is from ref. 16.

counterion disorder could ultimately suppress diffraction intensities for these two species, which failed to produce diffraction patterns despite producing crystal-like objects.

Single-crystal diffraction analyses of **1**, **2**, **5**, and **6** revealed similar molecular geometries (Fig. 3). All vanadium (IV) ions are six-coordinate, with average V–O bond distances ranging from 1.938(4) Å to 1.942(6) Å, as is common for this geometry and oxidation state. Furthermore, all molecules exist hydrogen-bonded to two *n*-Bu_3NH^+ cations through the O atoms of the catecholate ligands. This interaction holds the counterions at a similar distance from the V(IV) ion in all complexes as evidenced by an average V•••$HNBu_3^+$ distance of 2.969(4) Å. Finally, the six-membered catechol rings provide two sets of sites for ligand-based nuclear spins at the same distance from the V(IV) ion, either the 3 and 6 positions or the 4 and 5 positions. The average V•••X distances at these two sites, respectively, are 4.545(2) and 6.019(5) Å for V•••H and slightly longer 4.765(3) and 6.526(5) Å for V•••Cl. For comparison, these distances are all shorter than the analogous V•••Br distances in the brominated analogues, which are 5.04(1) Å for the 3,6 positions and 6.90(2) Å for the 4,5 positions.

Continuous-shape-measure analyses[41,42] were performed to test the extent to which the different chlorination patterns produced geometrical changes to V(IV) coordination shell. We tested the VO_6 coordination shells against both octahedral and trigonal prismatic geometries. Here, a shape measure of 0 corresponds to a perfect match for an octahedral geometry. Shape measures for the octahedral geometry were 1.7, 2.7, 4.5, and 2.7 for **1**, **2**, **5**, and **6**, respectively. Generally, deviations > 0.1 in the shape measure indicate distorted geometries. Thus, **1**, **2**, **5**, and **6** are all described as distorted octahedra. Note that the range of distorted values of **1-6** span the range of values for the Br-analogues (1.41 to 3.97),[17] and that the shape measure of **5** is larger than its brominated analogue (3.97). Hence, any possible magnetic effect due to a large deviation in the shape measure observed for that brominated species should also be present in **5**, if solely attribute to distortion away from O_h.

We also compared the ligand twist angles for **1**, **2**, **5**, **6** and the 4,5-dibromo analogue reported previously as this is another useful measure of distortion.[17] The twist angle, θ, is defined by the measured angle between the idealized C_3 axis of the V(IV) complex and the plane formed by the two ligand O atoms and the central V atom, as depicted in Fig. 4. The geometry is a regular octahedron if θ = 30°. The measured angles ranged from 18.62-29.63° indicating a

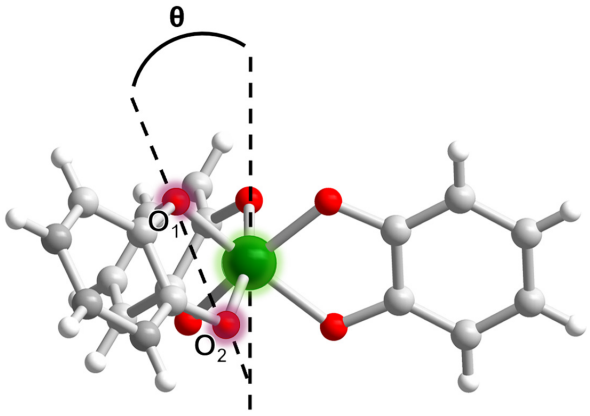

Figure 4. Visual depiction of twist angle measured for V(IV) complexes. The angle was measured from the *z*-axis of the metal ion and the two oxygens bonded to the metal ion.

distorted octahedral geometry for all complexes, in agreement with the shape measure (Table S4).[43] The 4,5-dihalo complexes exhibited the highest deviation of the series, with θ = 18.62° for the bromo analogue and θ = 18.67° for **5**. But there is a minimal, Δθ = 0.05° difference between them. Together with the shape measure scores, these structural analyses suggest that there are minimal geometric differences between **5** and its brominated analogue.

^{1}H Nuclear magnetic resonance analyses (400 MHz) of the prepared complexes and ligands reveal a wide range of peaks from a combination of the *J*-coupling, differing chemical shifts, and hyperfine interactions (Figs. 5, S11-S15). For the pure catechol ligands of **1-6**, ^{1}H δ values occur over a range of 7.0-6.7 ppm, or 36-63 Hz, for the asymmetric ligands, induced by aromatic *J*-coupling and differing chemical shifts. In contrast, for the symmetric ligands, ^{1}H peaks are relatively sharp, with a linewidth of 3-4 Hz. These observations are consistent with those made on brominated analogues.[17]

When complexed to the open-shell V(IV) ion, the ^{1}H NMR peaks shift and broaden consistent with the presence of hyperfine interactions with the $S = {}^1/_2$ metal (Figs. S5-S10). Importantly, assignment of the ^{1}H NMR spectra for open-shell complexes can be challenging, but in this case, our series of ligands and complexes enables us to conclusively assign peaks by substitution with Cl nuclei, which do not produce peaks in ^{1}H NMR. For example, **1-4**, which feature ^{1}H nuclei at the 4 and 5 positions of the catechol rings,

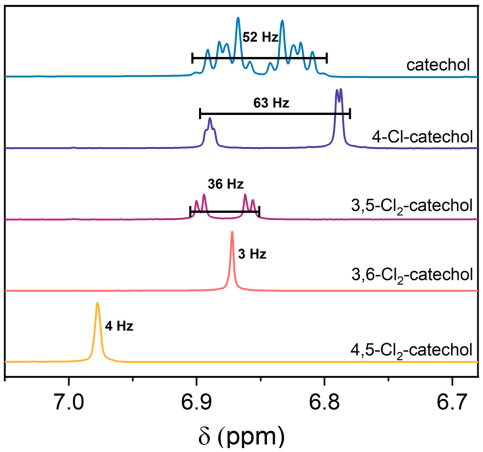

Figure 5. 400 MHz solution-phase ^{1}H NMR spectra of the individual catecholate ligands of **1**-**5**.

consistently and reproducibly yield peaks in the aromatic region of 6.8 to 7.6 ppm. These peaks are relatively broad, with average linewidths of ca. 130 Hz. Complex **5**, which has ^{1}H nuclei at the 3 and 6 positions of the ring, in contrast features no observable ^{1}H peaks (and **6**, which has no ligand ^{1}H nuclei, is silent in this regime). Thus, it appears that protons at the 3 and 6 positions of the ring are NMR silent under our conditions, possibly broadened into the baseline owing to proximity to the V(IV). In contrast, ^{1}H nuclei at the 4 and 5 positions of the catecholates are resolvable. These general observations are also made on the analogous Br-substituted complexes.[17]

Continuous-wave and echo-detected EPR spectra were recorded on **1**-**6** to study if and how the chlorination pattern affected the electronic structure of the molecule, and in particular, the spin density distribution over the metal and ligand (Figs. 6, S16-S18). Measurements were conducted in both solution and the solid state using X-band (ca. 9.46 GHz) and high-frequency (120 GHz) microwaves for **1**-**6**. The X-band solution and solid-state spectra show 8-line patterns that span ca. 100 mT, representative of hyperfine coupling of the $S = {}^{1}/_{2}$ V(IV) to the $I = {}^{7}/_{2}$ ^{51}V nucleus. The 120 GHz echo-detected spectra, in contrast, shows a single broad transition near 4.4 T. The enhanced effect of *g*-anisotropy and *g*-strain in the frozen solution leads to broad spectra at high field, which precludes direct observation of the hyperfine splitting in the 120 GHz spectra, though the accuracy of the *g* anisotropy is still relatively high.[44]

Simulation of all spectra was performed with Easyspin to extract the *g* and *A* values in the applied spin Hamiltonian:[45]

$$\hat{H} = g_e \mu_B B \hat{S} - g_N \mu_N B \hat{I} + \hat{I} A \hat{S} \quad (4)$$

Here, g_e and *A* correspond to rhombic electronic g factors and ^{51}V hyperfine coupling constants, respectively. $\hat{S}$ and $\hat{I}$ are electronic and nuclear spin operators, respectively, μ_B and μ_N are the Bohr and nuclear magnetons, respectively, and g_N the nuclear *g* factor for ^{51}V with *B* the magnetic field. Though ^{51}V is a quadrupolar nucleus, the quadrupolar coupling for this nucleus is generally small (< 1 MHz), and attempts to improve spectral simulations by inclusion of quadrupolar coupling were not successful.[46]

The resulting simulations for the data collected at X-band and 120 GHz reveal similar *g* and *A* values for both frequencies that do

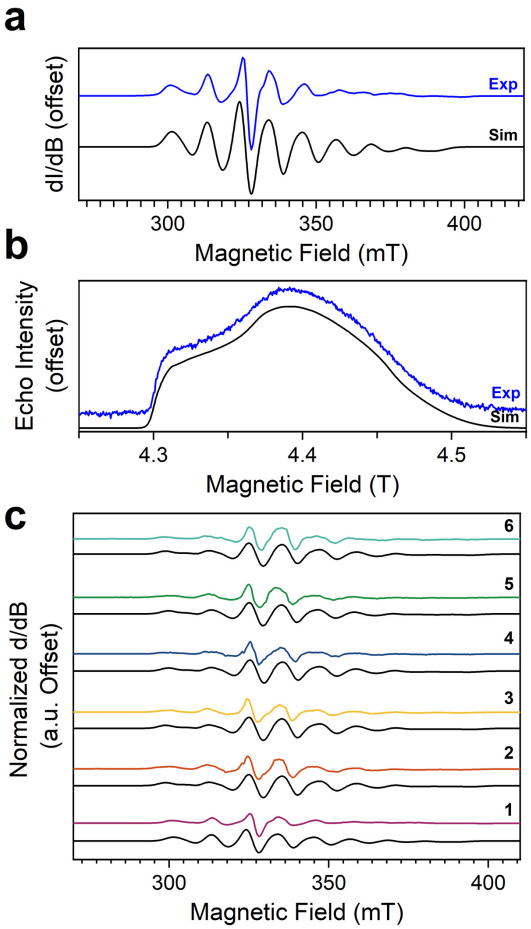

Figure 6. (**a**) X-band continuous-wave EPR spectrum of **1** (blue) at 100 K and simulation (black). Experimental details: 1 mM solutions; 0.63 microwave power; microwave frequency, *ca.* 9.46 GHz; modulation frequency, 100 kHz; modulation amplitude, 1.0 G; number of scans ranged from 10 to 15 to obtain good signal-to-noise ratios. (**b**) 120 GHz echo-detected, field-swept spectra of 1 mM of **1** in OTP solution (blue) at 5 K and simulation (black). (**c**) Frozen-solution X-band EPR spectra of **1**-**6**, presented side-by-side for comparison. Black lines are spectral simulations, colored lines are the experimental data. Instrumental parameters are the same across **1**-**6** and same as in panel **a**. See text and SI for simulation details.

not vary substantially as a function of ligand (Tables S5-S7). The *g* values of an open-shell metal ion are linked to the orbitals that are holding the unpaired electrons. Similarly, the magnitude and sign of *A* are also dependent on the orbital containing the spin, and, vitally, on the extent to which the spin is delocalized away from the nucleus engaged in the hyperfine coupling. Thus, the obtained *g* and *A* values indicate a consistent electronic (and physical) structure for V(IV) in **1**-**6**, with the unpaired electron localized on the V(IV) ion and no substantial changes in delocalization onto the ligands. We further note these values are also very close to those observed for the brominated analogues.[17] Finally, we note that good simulations of the solution-phase data can be made using these anisotropic *g* and *A* values and report solution-phase tumbling times for the complexes, which are ca. 400 ps and in the range expected for these species in this solvent.[14,16]

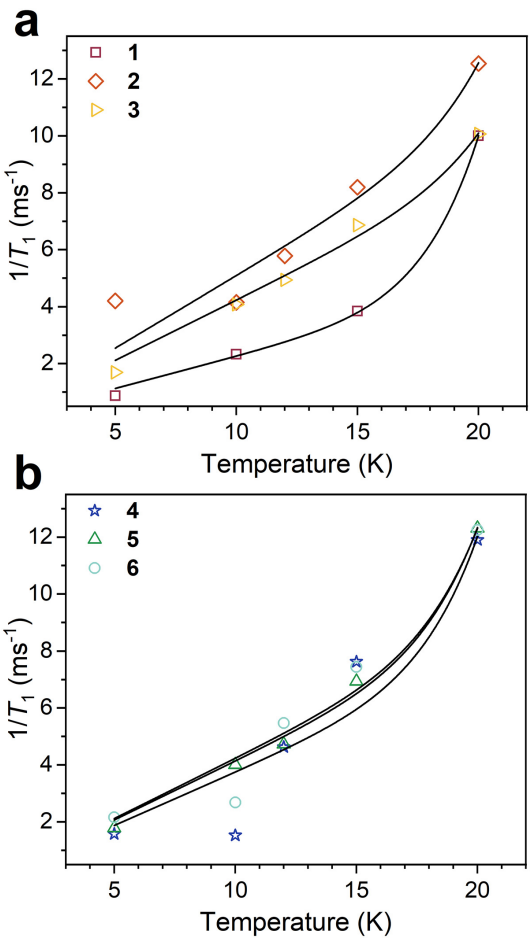

Figure 7. (**a**) Temperature dependence of the spin-lattice relaxation rate ($1/T_1$) for **1**-**3**. (**b**) Temperature dependence of the spin-lattice relaxation rate ($1/T_1$) for **4**-**6**. Simulation of the *T*-dependence is given as a black trace. Approx. field of acquisition was 4.4 T, the microwave frequency was 120 GHz, and samples were 1 mM in *o*-terphenyl. Fitting parameters and exact T_1 values are tabulated in the ESI. †

The first analysis of the impact of the chloro substitutions on the dynamic spin properties was performed by studying the spin-lattice relaxation times (T_1) for **1**-**6**, all at 120 GHz, as a function of temperature, from 5 to 20 K (Figs. 7, S19-S24). T_1 times, determined by inversion recovery experiments, varied between 1.15 ms and 0.1 ms over this window, generally decreasing with increasing temperature.

Analysis of the temperature dependence of T_1 (or the rate, $1/T_1$) enables a deeper look into the operative spin-lattice relaxation processes in **1**-**6**. Previously we hypothesized and reported a dominant direct method for the cause of shortening in T_1.[17] The dominant method is expected to be similar for this series due to similarities in structure and chemical composition. We found that the data for all complexes were readily modeled using a sum of direct and Raman processes, as shown in equation 2 (Fig. 7). The obtained parameters from modeling the T_1 data vary from **1**-**6** (Table S8), but do not do so substantially, and we note the relative paucity of the temperature points, suggesting care should be taken in confidence to the absolute values of these parameters. Nevertheless, T_1 mechanisms typically vary considerably between molecules with

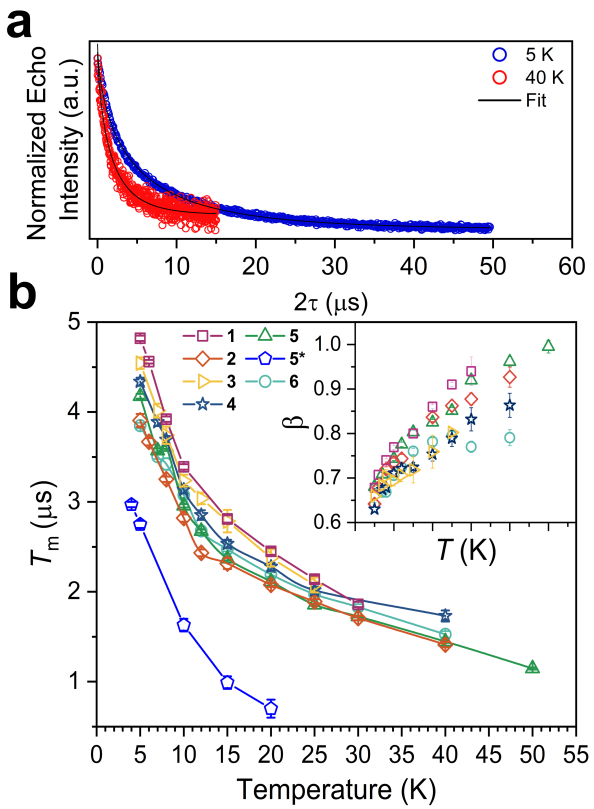

Figure 8. (**a**) Selected variable-temperature Hahn-echo decay curves (color traces) and fits (black traces) for **4**. (**b**) Variable-temperature T_m data for **1**-**6**. Data were collected at 120 GHz frequency on samples of *ca*. 1 mM concentration *o*-terphenyl glass. Data for the brominated analogue of **5**, here **5***, is also presented for clarity. Error values are generally within the width of the data symbols – exact uncertainties are tabulated in the ESI.†

differing electronic structures or local physical environments.6 Hence, the relative similarities in the fitted parameters for the relaxation mechanisms for **1**-**6** are consistent with the similarity in the *g* and *A* values and reflect the use of the same solvent matrix for measurement. Finally, we note that the range of T_1 values here is close to the brominated analogues reported by us earlier.[17]

Finally, we tested the impact of the different substitutional patterns of **1**-**6** on the phase memory relaxation times, T_m. To do so, we performed two-pulse Hahn-echo experiments at the field of highest echo intensity (ca. 4.4 T, Figs. 8, S27-S34). Echo intensities generally decay with increasing interpulse time, fading away completely by 50 μs at 5 K, but decaying far faster as temperatures increase (Fig. 7). Echo decay curves were collected until about 40-50 K for all complexes, at which temperature the long pulses (π/2 = 600 ns) made it challenging to observe an echo.

Extraction of T_m from the echo decay curves was performed by fitting the decays with a stretched exponential function, equation 4. T_m values collected in this manner are around 4-5 μs at 5 K for all complexes, then decrease sharply to about 2 μs with increasing temperature to 10 K. Above 10 K, T_m relatively slowly decreases with increasing temperature until the echo is no longer viable, about 40-50 K. These collected values of T_m are in the expected range of T_m for metal complexes at these fields. The β values extracted are ca. 0.6

for all complexes at 5 K and increase with increasing temperature to ca. 0.85 at 40 K (Fig. 8, inset). β values of this magnitude are common when instantaneous diffusion is an important mechanism for relaxation, as opposed to, e.g. librations or solvent-based spin diffusion.[11,22] Finally, we note that the T_m values are much lower than the obtained T_1 values, suggesting that T_m relaxation mechanisms are not strictly governed by spin-lattice relaxation. These observations are typical for V(IV) at the high-field and frequency of these measurements.[17,18]

To discern between these last possibilities, we tested the dependence of T_m on the π pulse length in the Hahn-echo sequence at 120 GHz. A strong dependence of T_m on this pulse length would indicate that instantaneous diffusion is integral to phase memory relaxation.[40] We collected echo decay curves at 5 K for **1**, **5**, and the 4,5-dibromocatechol analogue of **5**, $(Bu_3NH)_2[V(C_6H_2Br_2O_2)_3]$,[17] at 5 K using a two-pulse Hahn echo sequence with a varied π-pulse length from 100 to 600 ns (Fig. S35). Extracted T_m values from these experiments are in the same range as reported above and did not vary with π-pulse length. This invariance suggests that instantaneous diffusion is not the origin of the short β values and is consistent with the low concentrations of the analyzed samples.[38]

An important additional test, needed in followup to our prior report,[17] was the extent to which the R_3NH^+ counterions could be contributing to phase memory relaxation. Prior studies by some of us and others indicate that CH_3 groups can trigger shorter T_m values and produce smaller (< 1) β values in the Hahn-echo experiment at lower fields (ca. 3500 G) and lower frequencies (ca 9.5 GHz).[16,18] Just above, we disproved that the origin of the low values could be due to the instantaneous diffusion at high fields/frequencies. The counterion CH_3 groups are therefore another potential option, tests at high field and frequency had yet to be established.

We collected Hahn-echo decay data for **1**, **7**, and **8** at 120 GHz to test the role of counterion on T_m at high field/frequency for the first time (Figs. 9, S27,S33,S34). To do so, we performed two-pulse Hahn-echo experiments at the field of highest echo intensity (ca. 4.4 T for 120 GHz, Fig. S18-S17). The values of T_m at 5 K ranges from 3.62-4.04 μs for **1**, **7**, and **8**. These T_m values decrease slowly with increasing temperature, reaching 1.12-1.21 μs at 30 K for **1** and **7** respectively. The β values for the Hahn echo decays in these experiments are 0.6-0.7 for **1** and 7 and is 1.08 for 8 at 5 K. The β values for **1** and **7** approach 1 as the temperature increased to 30 K. The β for **8** does not change significantly as the temperature increases being 1.16 at 30 K.

Discussion

The foregoing results are significant for at least two reasons. First, we note that the effect of increasing chlorine on the ligand shell appears to be detrimental to T_m at 120 GHz. The effect is most evident upon comparison of **1** and **6**, where **1** has all protons and a higher T_m versus **6**, which has all chlorines in the ligand shell and a shorter T_m. $^{35/37}Cl$ has a relatively small magnetic moment (^{35}Cl: μ_N= 0.82 μ_N ; ^{37}Cl: μ_N= 0.68 μ_N).[20] The nuclear magnetic moments of $^{35/37}Cl$ are infact close to those of deuterium (μ_N = 0.86 μ_N), which is a common substitute for ^1H that produces larger T_m values.[11,12] One would expect, therefore, that Cl substitution of the ligand shell would encourage generally longer T_m values for the V(IV) ion compared to both bromine and hydrogen substitution, but comparison of **1** and **6** shows that the opposite occurs. Hence, the mechanisms governing T_m relaxation in the present molecules are likely more complex than those in species where deuteration categorically lengthens T_m.

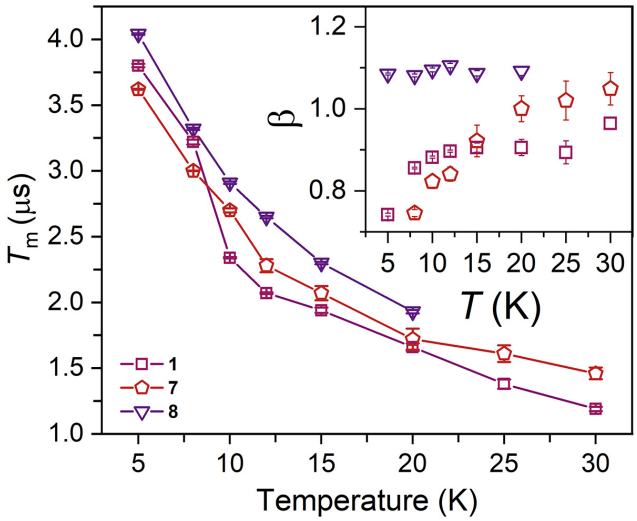

Figure 9. Variable temperature T_m data for **1**,**7**, and **8**. Data was collected at 120 GHz on samples of ca. 1 mM concentration *o*-terphenyl glass. Error values are generally within the width of the data symbols – exact uncertainties are tabulated in the ESI.†

Second, the presented data are interesting from the standpoint of Platt's scientific method of strong inference[47] because they disprove multiple hypotheses related to the anomalous short T_m of $[V(C_6H_2\text{-}4,5\text{-}Br_2O_2)_3]^{2-}$. Our initial hypothesis was that the short T_m for this species resulted from a symmetric ligand, which featured ^1H nuclei with precisely the same chemical shift and therefore efficient spin diffusion in the ligand shell. If this hypothesis were true, then **4** and **5** would both also show an anomalously short T_m. The ligand geometries are both symmetric in these complexes, and, like 4,5-dibromocatechol, the ^1H peaks are overlaid. But, neither compound has an anomalously short T_m. Hence, these results disprove that initial speculative hypothesis.

An additional alternative hypothesis is that a unique structural distortion in $[V(C_6H_2\text{-}4,5\text{-}Br_2O_2)_3]^{2-}$ was enabling short T_m values. If that were true, then some of the complexes in **1**-**6** would likely also show an abrupt T_m, as the structures of **1**-**6** and their brominated analogues all fall within the same window of shape measures and ligand twist angles expected for distorted octahedra. Hence, these results disprove that hypothesis. Additional evidence of the lack of this effect is found in the T_1 data, where changes in T_1 should follow significant structural distortion, but the T_1s for **1**-**6** and their brominated analogues are strikingly similar. This fact also seems to suggest no vibrational effects controlling T_1 or T_m, since the mass difference between $C_6H_4O_2^{2-}$ (FW = 108.09), $C_6Cl_4O_2^{2-}$ (FW = 245.88) and $C_6Br_4O_2^{2-}$ (FW = 423.68) is relatively large and all complexes have the same general molecular symmetry. A little caution here is likely warranted, as the molecular structures in the frozen solution samples are likely slightly different than those we observe by crystallography. However, we do note the consistency in the *g* anisotropy of the frozen-solution spectra, likely pointing toward similar molecular symmetries in the measurements.

Another important alternative hypothesis that is disproven is that the different bromine patterns could be modifying the way that the counterion is bound to the complex. Indeed, if a ligand were

enabling a counterion CH_3 group to approach the V(IV) more closely than the other ligands, earlier studies suggest a shorter T_m would result.[16,21] If the ligands played any substantial role in this effect whatsoever, then changing the counterion would produce a trend in T_m with the shorter V•••CH_3 distance producing a shorter T_m, as was observed at X-band frequencies. However, analysis of **1**, **7**, and **8** reveal a variation in T_m by *ca*. 0.3 μs at 120 GHz, which is unable to account for the 2 μs shift in T_m from $[V(C_6H_4O_2)_3]^{2-}$ to $[V(C_6H_2\text{-}4,5\text{-}Br_2O_2)_3]^{2-}$. Hence, our results seem to disprove the idea that the counterion could be the dominant contributor to T_m.

There are numerous other important findings from this study. First, we note generally small changes in hyperfine coupling and spin-lattice relaxation for **1**-**6**, while T_m varies by about 20 % as a function of number of $^{35/37}$Cl on the catechol. On a complex-to-complex comparison, there are no clear trends between any of those three parameters and the observed T_m trend.

We also note that the observed values for β are generally below 1 for **1**-**8** at the lowest temperatures but approached 1 as temperature was increased. A β value close to 2 indicates that spin diffusion amongst surrounding nuclei is causing T_m to be short.[45,48,49] Indeed, a relatively high β value for the complex $(Bu_3NH)_2[V(C_6H_2Br_2O_2)_3]$ was invoked in our prior arguments for ligand-based spin diffusion as the origin of effects of nuclear spin patterning.[17] In contrast, a β value below 1 indicates instantaneous diffusion or molecular librations/movement to be shortening T_m.[22] These general trends were established at X-band frequency. The presented data allow us to make two points about these trends at high field. First, the small β values are not from instantaneous diffusion. If they were, we would see a change in the T_m values for **1**, **5**, and $(Bu_3NH)_2[V(C_6H_2Br_2O_2)_3]$ with π pulse length, which we do not.[40] Our results also suggest that the low β values are not from the CH_3 groups in the counterions. At X-band frequency, β values ranges from 0.6 for **7** to 1.8 for **8**.[21] We do not see this same variation in our data for **1**, **7**, and **8**, which provides further evidence that the counterion is not controlling T_m at high field like it does at low field.

The final questions, then, are why $^{79/81}$Br nuclear spins have a particularly negative impact on the V(IV) T_m when at the 4,5-position v. $^{35/37}$Cl or ^{1}H, and why 4,5-dibromocatechol has a different impact on T_m in the V(IV) complexes versus tetrabromocatecholate, which also has $^{79/81}$Br nuclei at the 4 and 5 positions. Existing theory for the role of environmental nuclei in phase memory relaxation of an electron spin invoke a spin "flip-flop" action between pairs of nuclei near the electron spin which creates magnetic "noise" that causes T_m to be short. The probability of that nuclear pair undergoing the flip flop is greatest when the dipolar coupling between the pair of nuclei equals the difference in the two hyperfine couplings between the the nuclei and the nearby electronic spins.[50,51] The theory does not account for the quadrupolar couplings, Q, of the involved nuclei, which is 0 for ^{1}H, but much larger for Cl and Br atoms: ^{35}Cl Q = –81.65 mb, ^{37}Cl Q = –64.35 mb; ^{79}Br Q = 313 mb, ^{81}Br Q = 262 mb).[52,53] The theory does also not account for the spin dynamics (e.g. the T_1 or T_2) of the nuclei involved in the flip flop action, and T_1 and T_2 of the $^{35/37}$Cl and $^{79/81}$Br should be fairly short owing to their own intrinsic quadrupolar interactions and the proximate V(IV) ion.[52] We propose that some of these features could be impactful for governing the V(IV) T_m. It has been noted quadrupolar nuclei (e.g. $^{79/81}$Br) can drive ^{13}C nuclear spin relaxation,[54-56] and we tentatively propose that similar effects could also be a feature here. For all of the foregoing reasons, it would therefore be valuable to directly measure: (1) the V•••Br/Cl hyperfine interaction, (2) the chemical shifts of the Cl and Br atoms, and (3) the quadrupolar coupling of Cl and Br. These measurements are likely challenging because of the (1) the paramagnetic V(IV) ion and (2) the high quadrupolar couplings of the $^{35/37}$Cl and $^{79/81}$Br nuclei, which makes relaxation times fast and spectra broad. Nevertheless, we hope to report on said studies in the near future.

Conclusions

Deep understanding of the nature of spin-spin interactions and how they affect phase memory relaxation is essential in the longer picture of spin-based quantum applications of metal complexes. In this paper, we present a pulsed EPR and physical inorganic investigation of a set of eight V(IV) complexes with varying distributions of chlorine nuclear spins in the ligand shell and variable counterion size. The study disproves multiple hypotheses for the function of substitutional patterns of magnetic nuclei in governing relaxation. Hence, we are afforded new hypotheses related to the effects of fast-relaxing nuclei in the ligand shell. Future studies will test those hypotheses.

Author Contributions

R. M., C. E. J., Ö. Ü., and J.v.T. executed the syntheses and spectroscopic measurements. R. M. and J. M. Z. conceived of the experiments. All authors were involved in manuscript preparation.

Conflicts of interest

There are no conflicts to declare.

Acknowledgements

This research was performed with the support of Colorado State University (CSU), the National Science Foundation (CAREER award 2047325), and the Research Corporation for Scientific Advancement. We thank Dr. Samantha N. Macmillan at Cornell University for collecting the crystal structure of complex **6**. A portion of this work was performed at the National High Magnetic Field Laboratory, which is supported by the National Science Foundation Cooperative Agreement No. DMR-1644779 and the State of Florida.

Notes and references

§ In this paper, we use T_m to describe the time constant associated with the decay of the echo intensity in a Hahn-echo experiment. The parameter T_m is a broader, all-encompassing term for all relaxation processes that affect spin relaxation in the xy-plane. The T_m designation is particularly appropriate in this manuscript because there may be other factors controlling T_m (e.g. a short T_1) under the experimental conditions.

1 M. R. Wasielewski, M. D. E. Forbes, N. L. Frank, K. Kowalski, G. D. Scholes, J. Yuen-Zhou, M. A. Baldo, D. E. Freedman, R. H. Goldsmith, T. Goodson, M. L. Kirk, J. K. McCusker, J. P. Ogilvie, D. A. Shultz, S. Stoll and K. B. Whaley, *Nat. Rev. Chem.*, 2020, **4**, 490–504.
2 M. N. Leuenberger and D. Loss, *Nature*, 2001, **410**, 789–793.
3 E. Moreno-Pineda and W. Wernsdorfer, *Nat. Rev. Phys.*, 2021, **3**, 645–659.
4 K. P. Malikidogo, H. Martin and C. S. Bonnet, *Pharmaceuticals*, 2020, **13**, 436.
5 E. Coronado, *Nat. Rev. Mater.*, 2020, **5**, 87–104.

6 C. E. Jackson, I. P. Moseley, R. Martinez, S. Sung and J. M. Zadrozny, *Chem. Soc. Rev.*, 2021, **50**, 6684–6699.
7 D. Aravena and E. Ruiz, *Dalton Trans.*, 2020, **49**, 9916–9928.
8 J. M. Zadrozny, J. Niklas, O. G. Poluektov and D. E. Freedman, *ACS Cent. Sci.*, 2015, **1**, 488–492.
9 F.-S. Guo, B. M. Day, Y.-C. Chen, M.-L. Tong, A. Mansikkamäki, R. A. Layfield, *Science,* 2018, **362**, 1400-1403.
10 C. A. P. Goodwin, F. Ortu, D. Reta, N. F. Chilton and D. P. Mills, *Nature*, 2017, **548**, 439–442.
11 L. J. Berliner, G. R. Eaton and S. S. Eaton, *Distance Measurements in Biological Systems by EPR*, Springer US, 2002.
12 S. S. Eaton, G. R. Eaton and L. J. Berliner, *Biomedical EPR. Part A, Free radicals, Metals, Medicine and Physiology*, Springer, 2011.
13 J. P. Durrant, J. Tang, A. Mansikkamäki and R. A. Layfield, *Chem. Commun.*, 2020, **56**, 4708–4711.
14 C.-J. Yu, M. J. Graham, J. M. Zadrozny, J. Niklas, M. D. Krzyaniak, M. R. Wasielewski, O. G. Poluektov and D. E. Freedman, *J. Am. Chem. Soc.*, 2016, **138**, 14678–14685.
15 K. Bader, S. H. Schlindwein, D. Gudat and J. van Slageren, *Phys. Chem. Chem. Phys.*, 2017, **19**, 2525–2529.
16 C.-Y. Lin, T. Ngendahimana, G. R. Eaton, S. S. Eaton and J. M. Zadrozny, *Chem. Sci.*, 2019, **10**, 548–555.
17 C. E. Jackson, C.-Y. Lin, S. H. Johnson, J. van Tol and J. M. Zadrozny, *Chem. Sci.*, 2019, **10**, 8447–8454.
18 J. R. Weber, W. F. Koehl, J. B. Varley, A. Janotti, B. B. Buckley, C. G. Van de Walle and D. D. Awschalom, *J. Appl. Phys.*, 2011, **109**, 102417.
19 A. L. Falk, B. B. Buckley, G. Calusine, W. F. Koehl, V. V. Dobrovitski, A. Politi, C. A. Zorman, P. X.-L. Feng and D. D. Awschalom, *Nat. Commun.*, 2013, **4**, 1819.
20 J. R. Rumble, D. R. Lide and T. J. Bruno, *CRC Handbook of Chemistry and Physics: a Ready-Reference Book of Chemical and Physical Data*, CRC Press, Boca Raton, 99th edn, 2018.
21 C. E. Jackson, T. Ngendahimana, C.-Y. Lin, G. R. Eaton, S. S. Eaton and J. M. Zadrozny, *J. Phys. Chem. C*, 2022, **126**, 7169–7176.
22 A. Zecevic, G. R. Eaton, S. S. Eaton and M. Lindgren, *Mol. Phys.*, 1998, **95**, 1255–1263.
23 S. R. Cooper, Y. B. Koh and K. N. Raymond, *J. Am. Chem. Soc.*, 1982, **104**, 5092–5102.
24 C. Milsmann, A. Levina, H. H. Harris, G. J. Foran, P. Turner and P. A. Lay, *Inorg. Chem.*, 2006, **45**, 4743–4754.
25 B. Saikia, P. Borah and N. C. Barua, *Green Chem.*, 2015, **17**, 4533–4536.
26 G. M. Sheldrick, *Program for Empirical Absorption Correction of Area Detector Data*. SADABS 1996.
27 G. M. Sheldrick, *Acta. Cryst. A*, 2015, **71**, 3–8.
28 G. M. Sheldrick, *Acta. Cryst. C*, 2015, **71**, 3–8.
29 G. M. Sheldrick, *Acta. Cryst. A*, 2008, **64**, 112–122.
30 O. V. Dolomanov, L. J. Bourhis, R. J. Gildea, J. a. K. Howard and H. Puschmann, *J. Appl. Cryst.*, 2009, **42**, 339–341.
31 J. van Tol, L.-C. Brunel and R. J. Wylde, *Rev. Sci. Instrum.*, 2005, **76**, 074101.
32 G. W. Morley, L.-C. Brunel, J. van Tol, *Rev. Sci. Instrum.* 2008, ***79***, 064703.
33 Matlab; The MathWorks Inc.: Natick, MA, 2018.
34 Origin; OriginLab: Northampton, MA, 2018.
35 S. Stoll and A. Schweiger, *J.Magn. Reson.*, 2006, **178**, 42–55.
36 T. J. Pearson, D. W. Laorenza, M. D. Krzyaniak, M. R. Wasielewski and D. E. Freedman, *Dalton Trans.*, 2018, **47**, 11744–11748.
37 M. Atzori, S. Benci, E. Morra, L. Tesi, M. Chiesa, R. Torre, L. Sorace and R. Sessoli, *Inorg. Chem.*, 2018, **57**, 731–740.
38 T. Ngendahimana, R. Ayikpoe, J. A. Latham, G. R. Eaton and S. S. Eaton, *J. Inorg. Biochem.*, 2019, **201**, 110806.
39 R. Ward, A. Bowman, E. Sozudogru, H. El-Mkami, T. Owen-Hughes and D. G. Norman, *J. Magn. Reson.*, 2010, **207**, 164–167.
40 H.-J. Lim, S. Welinski, A. Ferrier, P. Goldner and J. J. L. Morton, *Phys. Rev. B*, 2018, **97**, 064409.
41 S. Alvarez, P. Alemany, D. Casanova, J. Cirera, M. Llunell and D. Avnir, *Coord. Chem. Rev.*, 2005, **249**, 1693–1708.
42 S. Alvarez, D. Avnir, M. Llunell and M. Pinsky, *New J. Chem.*, 2002, **26**, 996–1009.
43 D. L. Kepert, in *Progress in Inorganic Chemistry*, John Wiley & Sons Ltd. 1977.
44 D. Goldfarb and S. Stoll, *EPR Spectroscopy: Fundamentals and Methods*, Wiley, 2018.
45 Salikhov, K. M.; Tsvetkov, Y. D. *Time Domain Electron Spin Resonance*, Wiley, 1979.
46 S. Chicco, A. Chiesa, G. Allodi, E. Garlatti, M. Atzori, L. Sorace, R. D. Renzi, R. Sessoli and S. Carretta, *Chem. Sci.*, 2021, **12**, 12046–12055.
47 J. R. Platt, *Science* 1964, **146**, 347–353.
48 S. S. Eaton, G. R. Eaton and L. J. Berliner, Biomedical EPR. Part A, Free radicals, Metals, Medicine and Physiology, Springer, 2011.
49 A. Schweiger and G. Jeschke, *Principles of Pulse Electron Paramagnetic Resonance*; Oxford University Press, 2001.
50 E. R. Canarie, S. M. Jahn and S. Stoll, *J. Phys. Chem. Lett.*, 2020, **11**, 3396–3400.
51 S. M. Jahn, E. R. Canarie and S. Stoll, *J. Phys. Chem. Lett.*, 2022, **13**, 5474–5479.
52 C. M. Widdifield, R. P. Chapman and D. L. Bryce, in *Annual Reports on NMR Spectroscopy*, Academic Press, 2009, vol. 66, pp. 195–326.
53 W. C. Bailey and F. M. Gonzalez, *J. Mol. Struc.*, 2003, **651–653**, 689–695.
54 G. C. Levy, *J. C. S., Chem. Comm.*, 1972, 352–354.
55 A. Gryff-Keller, S. Molchanov and A. Wodyński, *J. Phys. Chem. A*, 2014, **118**, 128–133.
56 D. Kubica, A. Wodyński, A. Kraska-Dziadecka and A. Gryff-Keller, *J. Phys. Chem. A*, 2014, **118**, 2995–3003.

